Original Research

Correlation of Laminated MR Appearance of Articular Cartilage With Histology, Ascertained by Artificial Landmarks on the Cartilage

Dong Joon Kim, MD,[1] Jin-Suck Suh, MD,[1]* Eun-Kee Jeong, PhD,[1] Kyoo-Ho Shin, MD,[2] and Woo Ick Yang, MD[3]

The object of this study was to correlate the laminae of articular cartilage on magnetic resonance (MR) imaging with histologic layers. T1- and fast spin-echo T2-weighted images of articular cartilage with artificial landmarks were obtained under high gradient echo strength (25 mT/m) conditions and a voxel size of 78 × 156 × 2000 μm. Images were also obtained with a) changed frequency-encoding directions; b) changed readout gradient strength; and c) a varied number of phase-encoding steps. T2 mapping was performed with angular variations. Artificial landmarks allowed accurate comparison between the laminae on MR images and the histologic zones. No alterations of the laminae were noted by changing the frequency gradient direction. Altering readout gradient strengths did not show a difference in the thickness of the laminae, and increasing the phase-encoding steps resulted in a more distinct laminated appearance, ruling out chemical shift, susceptibility, and truncation artifacts. The T2 mapping profile showed an anisotropic angular dependency from the magic angle effect. In conclusion, the laminated appearance of articular cartilage on spin-echo and fast spin-echo MR images correlated with the histologic zones rather than MR artifacts. J. Magn. Reson. Imaging 1999;10:57–64.

Index terms: articular cartilage; magnetic resonance; magnetic resonance artifact

THE ARTICULAR CARTILAGE is subdivided histologically into superficial tangential, transitional, radial, and calcified cartilage zones according to the configuration of chondrocytes and collagen fibers. The long axis of the chondrocytes and the orientation of the collagen fibers are parallel to the articular surface at the superficial tangential layer and gradually reorient perpendicular to the articular surface at the radial zone (1). Recent advances in MR imaging techniques and the development of higher gradient hardware systems, even in clinical MR machinery, have made high-resolution imaging of such layers of the cartilage possible.

Accordingly, many reports on the MR imaging appearance of the articular cartilage and its correlation with the histologic zones are available. However, because of the lack of a definite landmark that would provide exact comparison between the histologic specimen and the MR image, the results differ (2–6). Moreover, conflicting reports suggest that the laminae visible on the images are due to MR artifacts and are not actual histologic layers (3,7,8).

The purpose of this study was to demonstrate the correlation of the laminated MR imaging appearance and histologic layers of articular cartilage by using artificial landmarks and also to rule out the possibility of MR artifacts.

MATERIALS AND METHODS

MR Imaging

Five V-shaped linear landmarks of different depths were artificially made parallel to the surface of bovine patella cartilage using a carving knife. The cartilage-bone block specimens were submerged in normal saline for 24 hours prior to imaging. All MR imaging was performed using a 1.5 T (Horizon, Echo speed, General Electric, Milwaukee, WI) system with a 3 inch surface coil. Before prescribing the MR sequences, the exact imaging plane was marked for an exact correlation with the histologic section. The imaging planes were perpendicular to the artificial linear landmarks. Common imaging parameters were as follows: field of view (FOV) 4 × 4 cm; matrix size 512 × 256 (display matrix size 512 × 512); slice thickness 2 mm; and number of excitations (NEX) 20. Both T1-weighted (TR/TE 300/14 msec) and fast spin-echo (FSE) T2-weighted (TR/TE 2000/53 msec) images were obtained after the specimen was placed with the surface parallel to the main magnetic field.

Imaging with changed frequency directions was performed on the T1-weighted study. On the T2-weighted study, supplemental images were obtained with the

[1]Department of Diagnostic Radiology, Research Institute of Radiological Science, Yonsei University College of Medicine, Seoul, Korea 120-752.

[2]Department of Orthopedic Surgery, Yonsei University College of Medicine, Seoul, Korea 120-752.

[3]Department of Pathology, Yonsei University College of Medicine, Seoul, Korea, 120-752.

* Address reprint requests to: J-S.S., Department of Diagnostic Radiology, Research Institute of Radiological Science, Yonsei University College of Medicine, 134 Shinchon-dong, Seodaemun-gu, Seoul, Korea 120-752. E-mail: jss@yumciris.yonsei.ac.kr

Presented in part at the 5th Annual Meeting of the International Society for Magnetic Resonance in Medicine, Vancouver, Canada, 1997.

Received

readout gradient doubled and halved. These parameters were controlled in the research mode (software version 5.3.4).

In a separate T2-weighted experiment with a different bovine patella specimen, five images were obtained with the phase-encoding step sequentially reduced from 256 to 128 in steps of 32. Other imaging parameters were identical to the above experiment.

With a third bovine patella specimen, we used an 8-echo spin-echo sequence modified by the authors from conventional multi-echo sequences to obtain the T2 values of the cartilage. T2 mapping was performed at 0°, 30°, 60°, and 90° angulation with the main magnetic field (B_o). Imaging parameters were as follows: FOV 8 × 4 cm; matrix size 512 × 256; slice thickness 2 mm; and NEX 20. TR was 2000 msec, and TE was varied, ranging from 15 to 120 msec in steps of 15 msec. Artificial landmarks were not made for the two specimens with sequentially reduced phase-encoding steps and T2 mapping.

Post-Processing

All image data (raw data) were transferred, displayed, analyzed, and post-processed in a Macintosh computer (Apple Computer, Cupertino, CA) using NIH IMAGE, a public-domain software package (version 1.62). The signal intensity (SI) profile from the surface of the cartilage to the bone marrow was measured twice, and the average value was used.

The images obtained with doubled and halved readout gradients were equally rescaled along the y-axis. A subtraction image of the rescaled images was obtained to compare the thickness of the laminae. A parametric T2 map of the cartilage was reconstructed on a pixel-by-pixel basis, using a linear square fit algorithm (9). The T2 map image was color encoded, and its value from the surface of the cartilage to the bone marrow was plotted.

Histologic Studies

After MR imaging, the corresponding sections of the specimen were fixed in formalin and then decalcified for 2–3 days. Hematoxylin & eosin, trichrome, Alcian blue, and Safranin O staining were performed for all sections. Light and polarized microscopic findings of the histologic specimen and the MR imaging findings were studied with the artificial landmarks as reference points in comparing the layers.

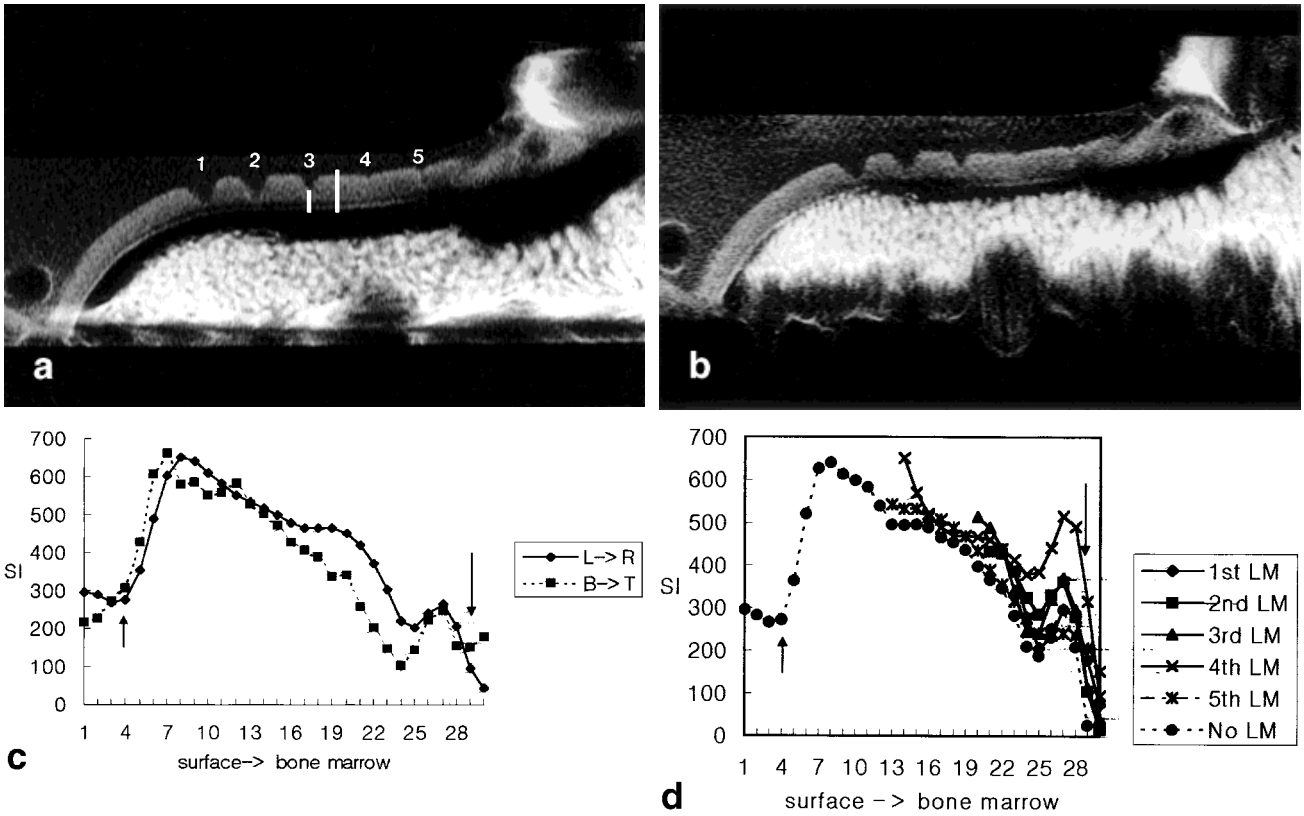

Figure 1. a,b: T1-weighted image of bovine patella with frequency-encoding direction from left to right and bottom to top, respectively. The five artificial landmarks are numbered. Cartilage shows a laminated signal intensity in both images. **c:** The signal intensity of the laminae from the surface (left arrow) inward to the calcified cartilage level (right arrow) at the site indicated in a (long vertical line) is plotted. Note that there is almost no shifting of the laminated appearance of the MR signals with changes in the frequency-encoding direction. L → R (diamonds) and B → T (squares) indicate right-to-left and bottom-to-top frequency-encoding direction. SI is the arbitrary number of the signal intensity. Numbers on the X-axis indicate the pixel depth from the surface through the bone marrow. **d:** The signal intensities of the laminae below the tip of each landmark are plotted. The left arrow indicates the superficial surface, and the right arrow indicates the calcified cartilage level. Each line represents the first (the deepest landmark [LM]) through the fifth (the shallowest landmark) landmarks and no artificial landmark.

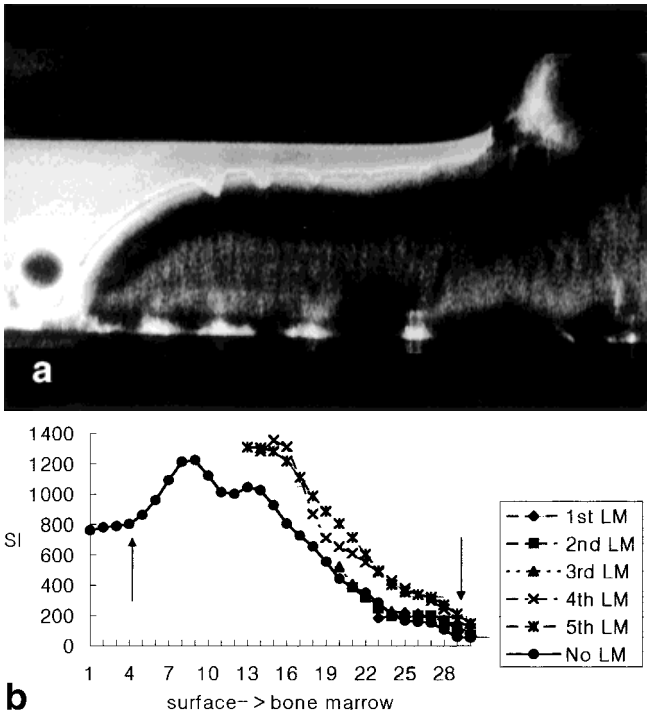

Figure 2. a: T2-weighted image of bovine patella with left-to-right frequency-encoding direction. **b:** The signal intensity of the laminae from the surface (left arrow) inward to the calcified cartilage level (right arrow) and below the tips of each landmark is plotted; a small peak is seen near the tip of the fourth deepest landmark (transitional layer). SI is an arbitrary number of the signal intensity. Numbers on the X-axis indicate the pixel depth from the surface through the bone marrow. Each line represents the first (the deepest landmark [LM]) through the fifth (the shallowest landmark) landmarks and no artificial landmark.

RESULTS

Laminated MR appearances of the articular cartilage were observed on MR images of both pulse sequences; these are clearly disclosed by the SI profile (Figs. 1, 2). On T1-weighted study, a high SI superficial layer with a gradually decreasing middle layer and an alternating band of low and intermediate SI in the deeper layer were noted. On T2-weighted study, the cartilage showed high and low SI layers with a second peak at a relatively superficial location (double peak) and SI gradually decreasing with depth (Fig. 2). Table 1 summarizes the MR imaging and histologic correlation results of the bovine T1- and T2-weighted images, respectively. The tangential and transitional zones on histologic specimens with a horizontal and mixed oblique orientation of the chondrocytes and collagen fibers corresponding to the fourth deepest landmark showed superficial high and superficial high and low SI on T1- and T2-weighted images, respectively. The upper radial zone with radial orientation of the chondrocytes and collagen fibers showed intermediate SI on T1-weighted image and high SI on T2-weighted image. At the histologic lower radial zone, well-defined low and intermediate SI bands were noted on the T1-weighted image just below the deepest landmark and above the tidemark zone. The calcified cartilage layer showed low SI on both pulse sequences (Figs. 1–3).

Table 1
Correlation (1:1) of Histologic Layers and Laminae on MR Images of Articular Cartilage

Histologic specimen	T1-weighted image	T2-weighted image
Tangential and transitional	Superficial high SI	Superficial high and low SI
Upper radial	Middle intermediate SI	Upper high SI
Lower radial	Low SI band Intermediate SI band	Lower intermediate SI
Calcified cartilage	Deep low SI	Deep low SI

SI profiles below the tip of each artificial landmark tended to show similar patterns, with slight variations. Changing the frequency and phase-encoding direction on the T1-weighted sequence did not alter the laminated appearance (Fig. 1).

Supplemental studies of T2-weighted images with altered readout gradients that were equally rescaled along the y-axis showed no difference in the thickness of the laminae (Fig. 4).

By decreasing the phase-encoding steps from 256 to 128 in steps of 32 on the T2-weighted sequence, the laminated appearance became less distinct, as is noted on the plotted graph (Fig. 5). No evidence of exaggeration of the laminated SI (peaks of SI) is noted with decreases in the phase-encoding steps.

T2 mapping of the bovine patella cartilage showed a double peaked appearance with a gradual decrease in between on the 0°, 30°, and 90° studies. The superficial peak showed a T2 value of 59.7 msec on the surface of the cartilage and a gradual decrease, with another peak having a T2 value of 97.1 msec at a lower layer on the 0° image. However, the 60° study showed a third peak between the first two peaks (Fig. 6).

DISCUSSION

The usefulness of MR imaging in the evaluation of articular cartilage in such disorders as chondromalacia (10), osteoarthritis (11), osteochondritis (12,13), and hemophilic and rheumatoid arthritis (14,15) is well established. Since the surface of the articular cartilage is avascular, repair of lesions localized to the cartilage surface by chondrocytes is very limited, but lesions reaching the subchondral plate are healed with fibrocartilaginous tissues such as vascularized tissues. Therefore, the depth of a lesion involving articular cartilage is important in making therapeutic decisions (16). Recently, high-resolution imaging using delicate hardware and imaging techniques for clinical MR machinery has raised more hope for a highly accurate diagnostic method for such cartilaginous lesions.

Modl et al (3) observed a trilamina appearance of human knees and ankles on T2-weighted image and correlated the laminae with the histologic zones using a thickness-percentage method as follows: the superficial lamina of low SI corresponded roughly to the tangential zone; the middle lamina of high SI corresponded to the

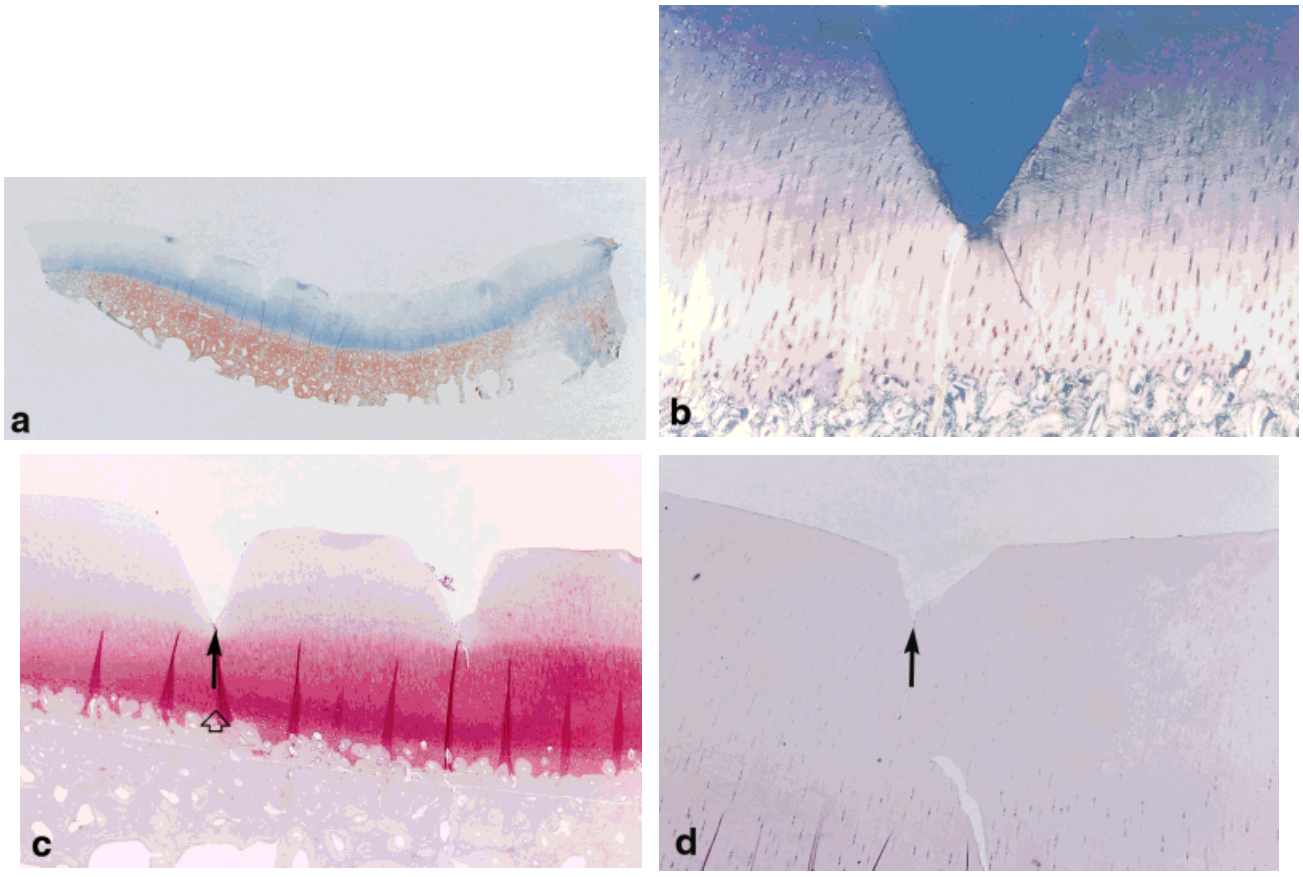

Figure 3. Histologic specimens of bovine cartilage with (**a**) trichrome (×10), (**b**) polarized microscope (×100), (**c**) Safranin O (×40), and (**d**) Alcian blue (×100). **a:** Five V-shaped landmarks are noted on the surface of the cartilage. Collagen fibrils are not clearly delineated, but staining becomes more intense with increasing depth. **b:** The orientation of collagen fibers is clearly visualized on this polarized microscope study. The tip of the deepest landmark is located above the lower radial zone, where the orientation of the collagen fibers is vertical. **c:** The tip of the deepest landmark is indicated (large arrow). The tidemark zone (open arrow) is seen. **d:** The fourth landmark (small arrow) is located at the transitional layer.

transitional zone; and a broad band of deep low SI corresponded to the deep radial and calcified cartilage zone.

Rubenstein et al (6) explained the trilamina appearance of bovine knees on T1-weighted images on the basis of the magic angle effect from different orientations of collagen fibers with respect to the static magnetic field. This resulted in anisotropic T2 in each histologic zone and gave a laminae correlation as follows: the superficial high SI corresponded to the tangential, transitional, and upper radial zone; the middle low SI corresponded to the bulk of the radial zone; and the deep intermediate SI lamina corresponded to the lower radial zone.

Many reasons for the varying SI of each lamina on MR images have been suggested, including differences in water content, differences in proteoglycan content (4), the magic angle effect of collagen fibers (6,17), and MR artifacts such as susceptibility, chemical shift, and truncation artifacts (8).

Chemical shift and susceptibility artifacts as a cause of the laminae in some of the images were a concern in this study. Chemical shift and susceptibility artifacts are most prominent when the laminae on images are perpendicular to the direction of the frequency-encoding gradient. However in our study, the laminae of the cartilage obtained after exchanging frequency- and phase-encoding directions on T1-weighted study showed little accentuation or alterations on the MR images, although fat in the marrow showed noticeable shifting according to the frequency-encoding directions (Fig. 1).

Another method we used to rule out susceptibility artifact was acquiring supplemental images with doubled and halved readout gradients (18). The following equation shows that the distance in shifting from susceptibility artifact is inversely proportional to the readout gradient:

$$Z \propto B_0 \cdot X / Gx$$

where Z = distance of shift, X = susceptibility difference between laminae, B_0 = magnetic field strength, and Gx = readout gradient.

If the laminae of the cartilage were from susceptibility artifacts, the thickness of the cartilage on equally rescaled images should show a fourfold difference between the doubled and halved readout gradient images. However, no definite difference in the thickness of the laminae was noted, and the laminae were almost can-

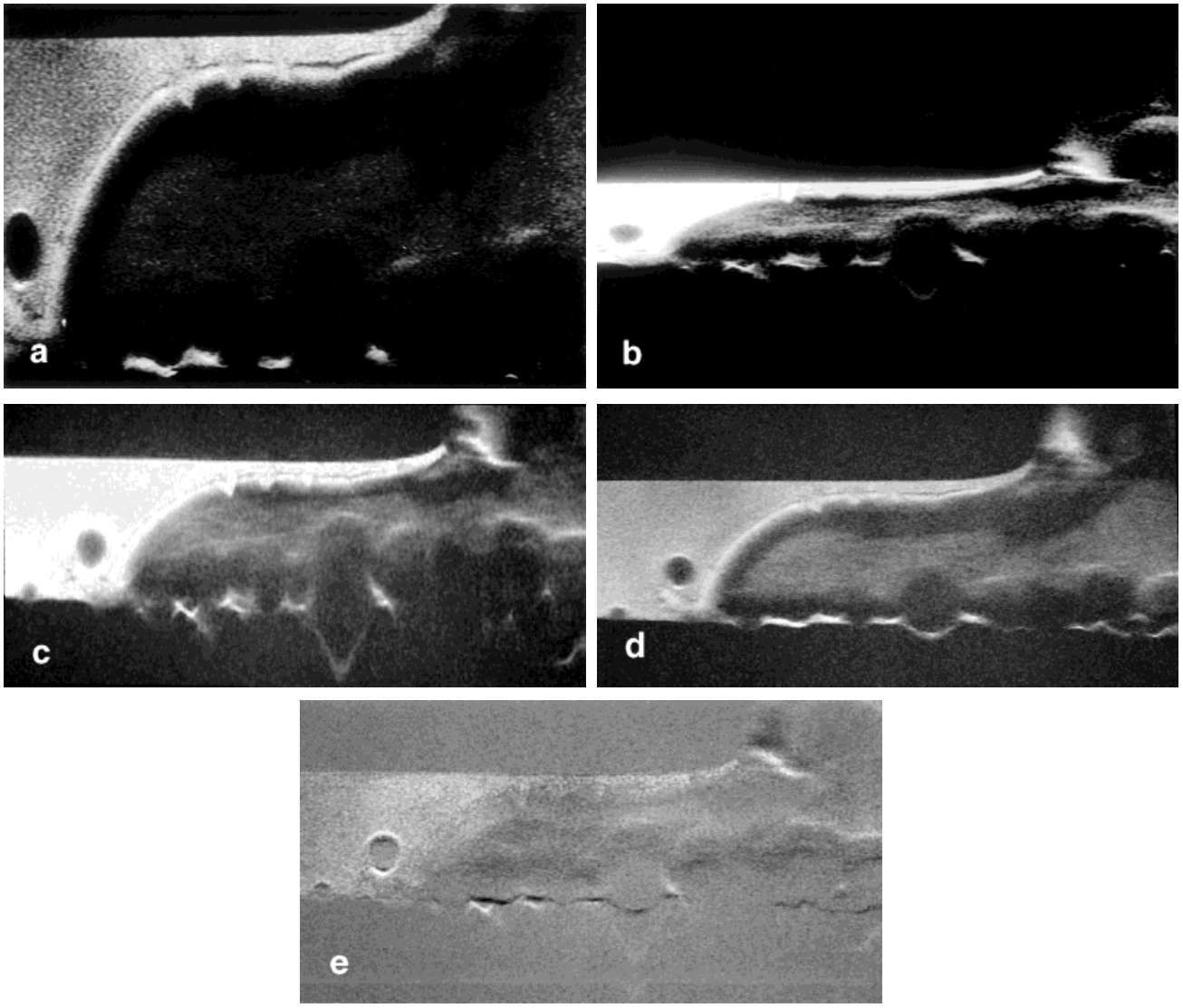

Figure 4. Bovine patella T2-weighted image with readout gradient doubled (**a**) and halved (**b**). The height of the patella sample shows a fourfold difference between the two images. The equally rescaled images of doubled (**c**) and halved (**d**) readout gradients and the subtraction image (**e**) of c and d show that the laminae are almost completely cancelled out.

celled out on the subtraction images, ruling out the possibility of susceptibility artifacts (Fig. 4).

Truncation artifacts as a cause of the laminated appearance of articular cartilage using fat-suppressed three-dimensional spoiled gradient-recalled sequences have been suggested (8). Truncation artifacts occur at surfaces with a large SI difference due to inadequate sampling. If the laminae in our study were from truncation artifacts, the SI profile (laminae) would have shown a shift on the plotted diagram. However, the laminae did not show any shifting on the plotted diagram. Also, they showed a more distinct laminated appearance as the phase-encoding steps increased, thereby ruling out truncation artifacts as the cause of the laminated appearance on fast spin-echo images (Fig. 5).

On the 0°, 30°, and 90° T2 mapping study, a gradual decrease from a superficial peak in T2 value was noted from the superficial surface to the subchondral bone layer, with another peak in the deeper layer. This double peak with a gradual decrease in between pattern in T2 values corresponds to the fact that the concentration of water gradually decreases inward (19). Moreover, the T2 mapping of the 60° study showed a third peak between the first two peaks, indicating angular anisotropy of water molecules along the collagen fibers (Fig. 6). The results of our study agree with prior studies noting that the magic angle effect is most prominent when the angle between the collagen fibers and B_0 is 55°. The SI profile of the T2-weighted image with a 512×256 matrix from the study with varied phase-encoding steps showed a similar pattern with the plotted T2 map at 0° angulation, indicating the importance of water content in the laminated appearance of the articular cartilage (Figs. 5, 6). However, the plotted graph was not so similar in the fast spin-echo T2-weighted study with a different specimen, even though there was a double peaked appearance at a more superficial location (Fig. 2). This may be the result of specimen-to-specimen dependent differences in the structural organization of cartilage tissue according to its maturity (20). The use of a fast spin-

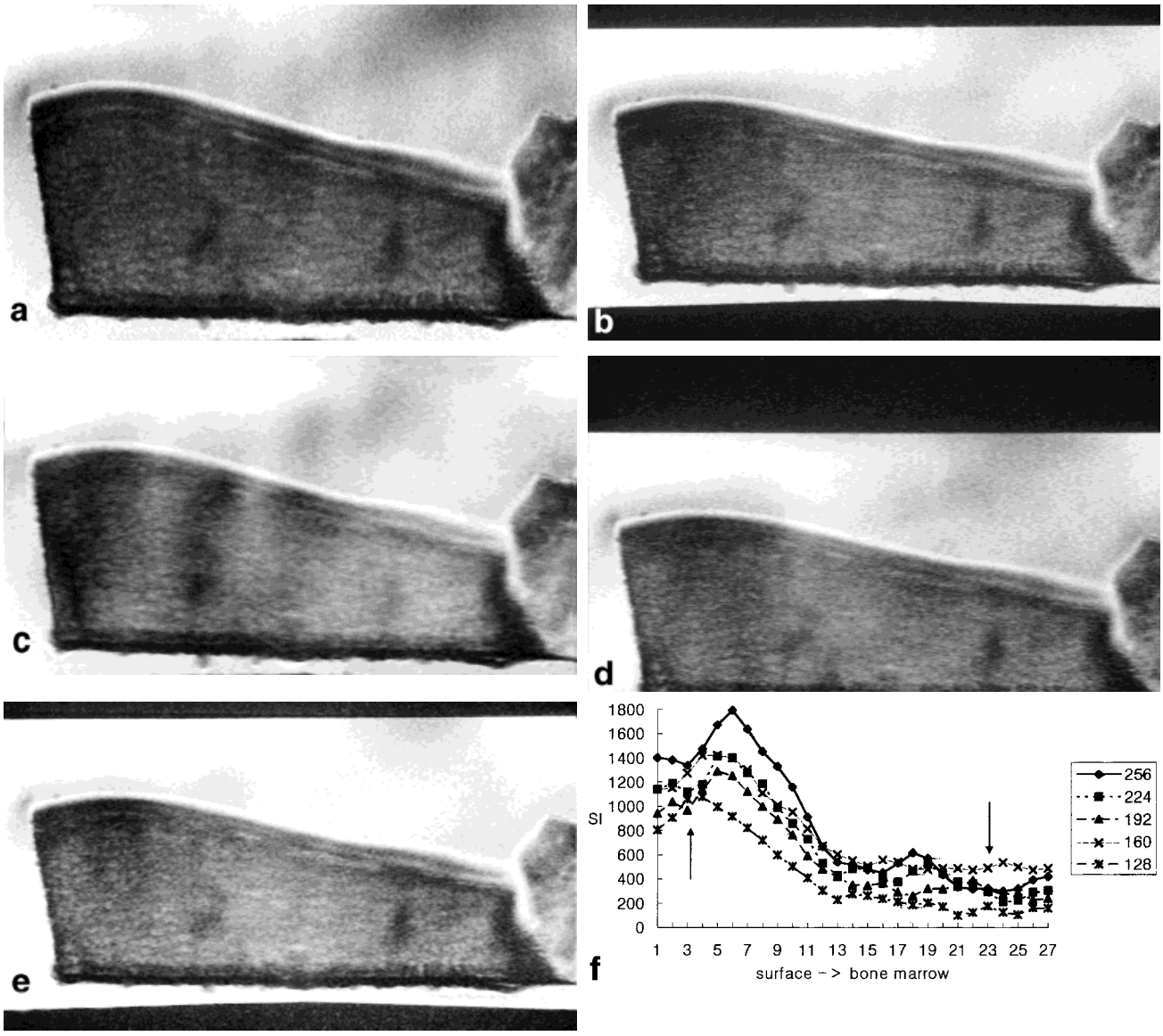

Figure 5. a–e: The T2-weighted images with the phase-encoding steps gradually decreased from 256 to 128 in steps of 32. **f:** The signal intensity of T2-weighted images versus the depth of the cartilage. The left arrow indicates the surface of the cartilage, and the right arrow indicates the calcified cartilage layer. Each line indicates varied phase-encoding steps, which are sequentially reduced from 256 to 128 in steps of 32.

echo instead of a conventional spin-echo sequence may have been another possible cause.

Our depth-related landmarks indicated the histologic layers directly, without influence from artifacts or misregistration of SI. However, correlation of the laminae on MR images with histologic layers was limited because there was no clear-cut border between the four histologic layers. The authors tried to overcome this limitation by using four different staining methods and polarized microscopy. Besides H&E, special stains such as trichrome were used for collagen-specific staining. Cationic dyes such as Alcian blue and Safranin O were used for the evaluation of proteoglycan components in the articular cartilage (21,22). (Each of these proteoglycan molecules is composed of a central protein core to which glycosaminoglycan chains are covalently bound.) The staining methods that best correlated the histologic layers with the laminae on MR images from chondrocyte morphology and orientation of collagen fibers or the matrix components were selected for comparison. A distinct linear low and intermediate SI band was noted below the deepest landmark at the histologic lower radial zone on the T1-weighted study; this band correlated with a distinct intensely staining layer on repeated Alcian blue and Safranin O stains, distant from the tidemark zone (Fig. 3). The collagen-specific trichrome stain also showed a deeper stain in the deeper layers, although not as distinct as the proteoglycan-specific stains. This can only be explained by the fact that the concentration of proteoglycans and collagen in the matrix of the cartilage increases from the articular surface inward in terms of depth from the surface of the articular cartilage (1). However, to our knowledge, there are no references in the literature showing such a

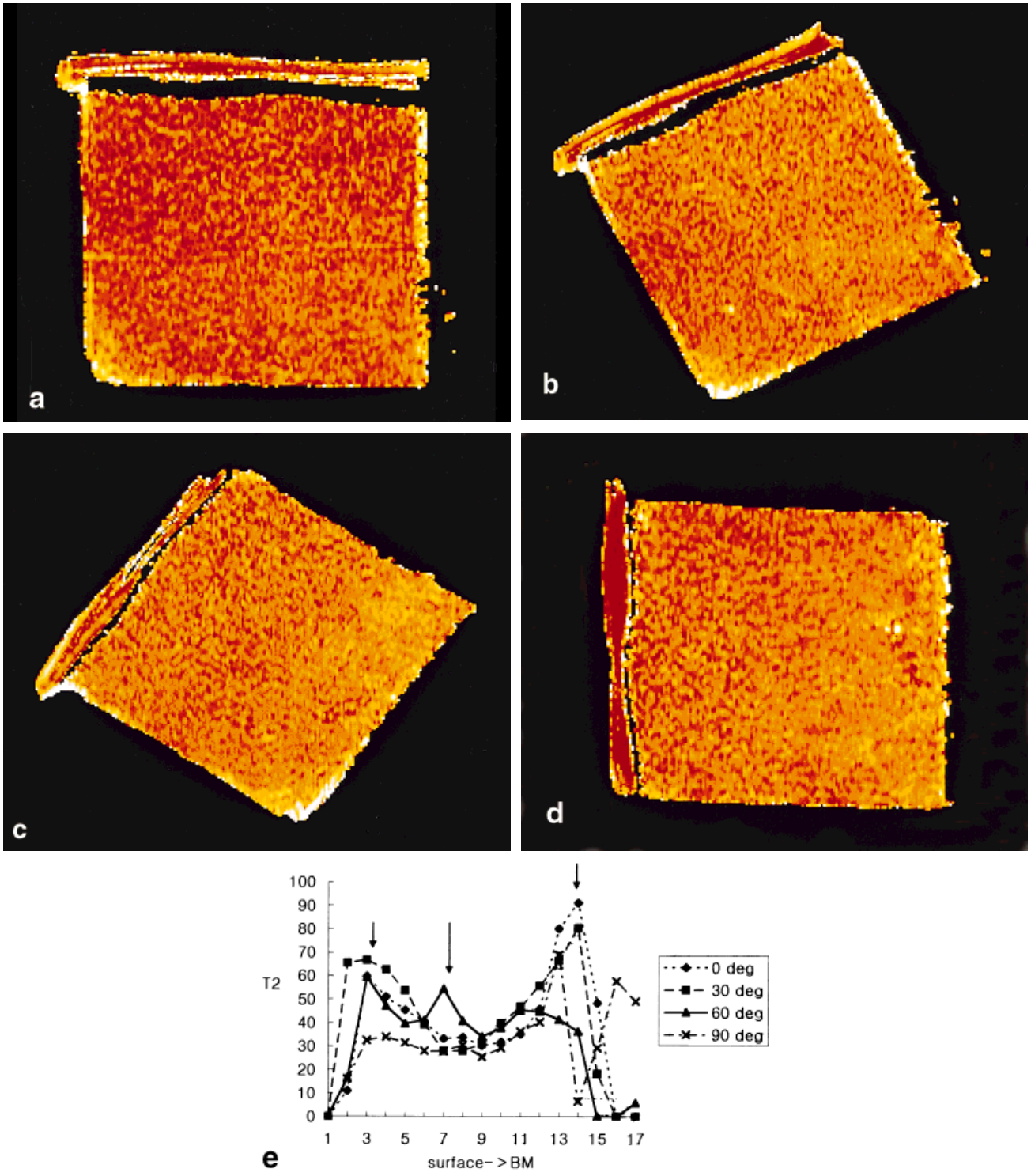

Figure 6. The color-coded T2 map images of 0° (**a**), 30° (**b**), 60° (**c**), and 90° (**d**) angles between the cartilage-bone block and B_o. **e:** Plotted graph of T2 values using four angles from the superficial to the deeper layers of the cartilage. Note the double peak (short arrows), with a gradual decrease in between, and a third peak (long arrow) in between the first two peaks on the 60° study. The T2 values are in milliseconds.

distinct layered difference in the distribution of proteoglycans, or any other components of the articular cartilage. Proteoglycans in the cartilage show their highest concentration around the immediate vicinity of chondrocytes designated the territorial matrix. The interterritorial matrix between cells and cell clusters shows a lower concentration of proteoglycans (1).

In mammals, about 90–95% of the collagen of normal articular cartilage consists of type II collagen; the remaining portion consists of type V, IX, X, and XI

collagens. Type II collagen provides a fibrillar network for the cartilage matrix and plays a major role in magnetization transfer contrast (23).

Slight baseline shifts of SI were noted between the original SI profile adjacent to the landmark and SI profile below the tip of the landmarks, as well as in the study with varied phase-encoding gradients. This is most likely from an inborn error of MR signal acquisition, of which the authors are currently unaware. The heat produced by carving out the artificial landmarks or differences in texture of cartilage, smooth at intact surfaces and irregular at carved out surfaces, may have altered the water diffusion capabilities in the immediate vicinities of the landmark and may also be responsible for the slight baseline shifts of SI measured below the tip of the landmarks.

The difference in the number of pixels from the surface of the cartilage to the calcified cartilage on the SI profiles, which varied roughly from 18 on the T2 map study and 32 on the T1- and T2-weighted studies, is most likely from differences in pixel size—156 × 156 μm (8 × 4 cm FOV, 512 × 256 matrix) and 78 × 156 μm (4 × 4 cm FOV, 512 × 256 matrix), respectively—and also from influences of differences in cartilage specimens.

One of the weaknesses of this study was that a fast spin-echo T2-weighted sequence was used for the sake of a shorter imaging time instead of a conventional T2-weighted spin-echo sequence. The limitations of a 1.5 T system for high-resolution and high signal-to-noise ratio imaging restricted visualization of the lamina splendens, a thin lamina devoid of collagen fibers (24). However, the sequences that were used in this study on a 1.5 T system could be potentially optimized and applied in high-resolution imaging in in vivo clinical settings.

In conclusion, the laminae of different SI were correlated with the histologic zones using artificial landmarks. We suggest that water content, represented by T2 value differences, as well as the amount of proteoglycan and collagen, contributes to the laminated appearance. Susceptibility, chemical shift, and truncation artifacts were ruled out as the cause of laminae on spin-echo and fast spin-echo MR images.

REFERENCES

1. Hunziker EB, Herrmann W. Ultrastructure of cartilage. In: Bonucci E, Motta PM, editors. Ultrastructure of skeletal tissues. Boston: Kluwer Academic Publishers; 1990. p 79–109.
2. Lehner KB, Rechl HP, Gmeinwieser JK, Heuck AF, Lukas HP, Kohl HP. Structure, function and degeneration of bovine hyaline cartilage: assessment with MR imaging in vitro. Radiology 1989;170:495–499.
3. Modl JM, Sether LA, Haughton VM, Kneeland JB. Articular cartilage: correlation of histologic zones with signal intensity at MR imaging. Radiology 1991;181:853–855.
4. Paul PK, Jasani MK, Sebok D, Rakhit A, Dunton AW, Douglas FL. Variation in MR signal intensity across normal human knee cartilage. J Magn Reson Imaging 1993;3:569–574.
5. Recht MP, Resnick D. MR imaging of articular cartilage; current status and future directions. AJR 1994;163:283–290.
6. Rubenstein JD, Kim JK, Morava-Protzner I, Stanchev PL, Henkelman RM. Effects of collagen on MR imaging characteristics of bovine articular cartilage. Radiology 1993;188:219–226.
7. Erickson SJ, Waldschmidt JG, Czervionke LF, Prost RW. Hyaline cartilage: truncation artifact as a cause of trilamina appearance with fat suppressed three dimensional spoiled gradient recalled sequences. Radiology 1996;201:260–264.
8. Frank LR, Brossman J, Bucton RB, Resnick D. MR imaging truncation artifacts can create a false laminar appearance in cartilage. AJR 1997;168:547–554.
9. Press WH, Teukolsky SA, Vetterling WT, Flannery BP, editors. Modeling of data. In: Numerical recipes in C—the art of scientific computing, 2nd ed. Cambridge: Cambridge University Press; 1992. p 656–706.
10. Yulish BS, Monimez J, Goodfellow DB, Bryan PJ, Mulopulos GP, Modic MT. Chondromalacia patella: assessment with MR imaging. Radiology 1987;164:763–766.
11. Konig H, Sauter R, Deimling M, Vogt M. Cartilage disorders: comparison of spin-echo, CHESS and FLASH sequence MR images. Radiology 1987;164:753–758.
12. Lehner K, Heuck A, Rodammer G, Raff W, Haller W. MRI bei der osteochondrosis dissecans. ROFO 1987;147:191–196.
13. Yulish BS, Mucopulos GP, Goodfellow DB, Bryan PJ, Modic MT, Dollinger BM. MR imaging of osteochondral lesions of talus. J Comput Assist Tomogr 1987;11:296–301.
14. Yulish BS, Lieberman AJ, Newman AJ, Bryan PJ, Mulopulos GP, Modic MT. Juvenile rheumatoid arthritis: assessment with MR imaging. Radiology 1987;165:149–152.
15. Yulish BS, Lieberman AJ, Szandjord SE, Bryan PJ, Mulopulos GP, Modic MT. Hemophilic arthropathy: assessment with MR imaging. Radiology 1987;164:759–762.
16. Sisk DT. Knee injuries. In: Crenshaw AH, editor. Campbell's operative orthopaedics. St. Louis: Mosby-Year Book; 1992. p 1487–1733.
17. Gründer W, Wagner M, Werner A. MR-microscopic visualization of anisotropic internal cartilage structures using the magic angle technique. Magn Reson Med 1998;39:376–382.
18. Lüdeke KM, Roschmann P, Tischler R. Susceptibility artefacts in NMR imaging. Magn Reson Imaging 1985;3:329–343.
19. Xia Y, Farquhar T, Burton-Wurster N, Ray E, Jelinski LW. Diffusion and relaxation mapping of cartilage-bone plugs using microscopic magnetic resonance imaging. Magn Reson Med 1994;31:273–282.
20. Hunziker EB. Articular cartilage structure in humans and experimental animals. In: Kuettner KE, Schleyerbach R, Peyron JG, Hascall VC, editors. Articular cartilage and osteoarthritis. New York: Raven Press; 1991. p 183–200.
21. Ippolito E, Pederini VA, Pederini-Mille A. Histochemical properties of cartilage proteoglycans. J Histochem Cytochem 1983;31:53–61.
22. Shepard N, Mitchell N. The localization of proteoglycan by light and electron microscopy using safranin O—a study of epiphyseal cartilage. J Ultrastruct Res 1976;54:451–460.
23. Seo GS, Aoki J, Moriya H, et al. Hyaline cartilage: in vivo and in vitro assessment with magnetization transfer imaging. Radiology 1996; 201:525–530.
24. Jeffery AK, Blunn GW, Archer CW, Bentley G. Three dimensional collagen architecture in bovine articular cartilage. J Bone Joint Surg [Br] 1991;73-B:795–801.